[3] A. Safaai-Jazi and G. L. Yip, "Cutoff Conditions in three layer cylindrical dielectric waveguides," *IEEE Trans. Microwave Theory Tech.*, vol. MTT-26, pp.898–903, Nov. 1978.
[4] J. A. Stratton, *Electromagnetic Theory.* New York: McGraw–Hill, 1941, ch. VI, pp. 372–374.

✤

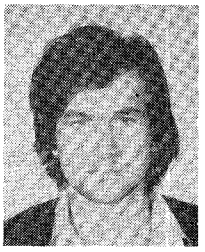

Nicholas M. Metrou was born in Ioannina, Greece, on October 5, 1957. He received the Diploma Degree (electrical engineering) from the National Technical University of Athens, in 1980 and has, since then, been following a course in Systems and Control, leading to the M.Sc. degree.

✤

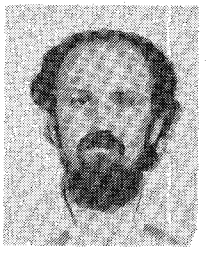

John D. Kanellopoulos was born in Athens, Greece, on December 12, 1948. He received the Diploma of Mechanical and Electrical Engineering and the Dr. Eng. degree from National Technical University of Athens (N.T.U.A.) in 1971 and 1979, respectively. He has also received the D.I.C. and Ph.D. degrees from Imperial College of Science and Technology, University of London, in 1979.

From November 1979 he has been an instructor in the Department of Electrical Engineering, National Technical University of Athens. His area of interests are electromagnetic scattering, millimetric wave propagation through rain media, and waveguide theory.

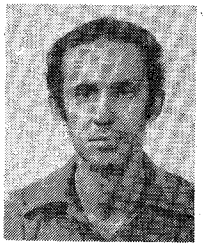

John A. Roumeliotis was born in Corinth, Greece, on January 2, 1953. He received the Diploma of E.E. and M.E. and the Dr. Eng. degree from the National Technical University of Athens, Greece, in 1975 and 1979, respectively. From 1979 to 1981, while doing his military service, he worked in the Hellenic Air Force Research Center.

His main fields of interest include scattering, waveguide propagation, and boundary value problems in electromagnetic theory.

✤

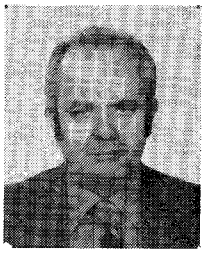

John G. Fikioris was born in Sparta, Greece, on April 9, 1931. He received the Diploma of E.E. and M.E. from the National Technical University of Athens, Greece, in 1955. He received the M.S.E.E. degree from Rensselaer Polytechnic Institute, Troy, NY, in 1958, and the M.A. and Ph.D. degrees in applied physics from Harvard University, Cambridge, MA, in 1963.

From 1962 until early 1966, he worked as a Research Scientist with the RAD division of Avco Corporation, Wilmington, MA. From January 1966 to June 1972, he was Professor of Electrical Engineering at the University of Toledo, OH. In May 1972, he was elected Professor of Wireless and Long Distance Communications at the National Technical University of Athens, a position that he holds to date. His main fields of interest include guiding phenomena, wave optics, antennas and wave propagation, diffraction and scattering, boundary value problems in potential and electromagnetic theory and applied mathematics.

Dr. Fikioris is a member of Sigma Xi.

Ridged Waveguides for Ultra-Broad-Band Light Modulators

GOTTFRIED MAGERL, MEMBER, IEEE, AND PETER W. FROEHLING

Abstract—**The electromagnetic field of the dominant mode propagating in the inhomogeneously dielectrically loaded double ridged waveguide is given in terms of a modal series expansion. The numerical evaluation of the propagation constant reveals a remarkably linear dispersion diagram in close agreement with measurements performed in the 8–40-GHz range. Based on this analysis, the bandwidth of a ridged waveguide CO_2-laser modulator is calculated to exceed 40 GHz, when a 25-mm long CdTe crystal is used as electrooptic material.**

Manuscript received June 17, 1981; revised October 15, 1981. This work was supported by the Fonds zur Forderung der wissenschaftlichen Forschung, Wien, Austria.

G. Magerl is with the Department of Chemistry, University of Chicago, Chicago, IL 60637, on leave from the Institut fur Nachrichtentechnik, Technicshe Universitat Wien, Gusshausstrasse 25, A-1040 Wien, Austria.

P. W. Froehling is with the Institut fur Nachrichtentechnik, Technicshe Universitat Wien, Gusshausstrasse 25, A-1040 Wien, Austria.

I. Introduction

ELECTROOPTICALLY mixing a fixed-frequency CO_2 laser with a frequency-tunable microwave signal yields continuously tunable laser sidebands in the infrared. In this way, the tunability of the microwave signal is transferred to the IR wavelength region from about 9–11 μm. Moreover, the accurate sideband frequency can be de-

0018-9480/82/0200-0220$00.75 ©1982 IEEE

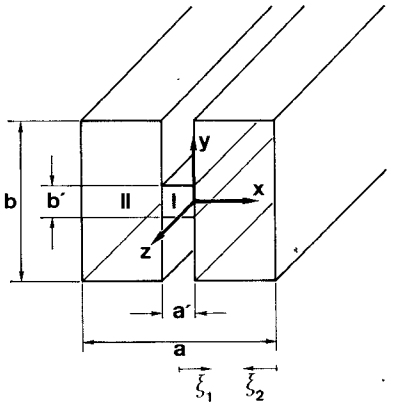

Fig. 1. Cross section of inhomogeneously dielectrically loaded double ridged waveguide. When employed as a light modulator, the laser beam is focused in z-direction through the electrooptic crystal (region I), whereas region II of the cross section remains empty.

termined as sum or difference of tabulated laser line frequency [1] and of measured microwave frequency. Therefore, laser sidebands have become a favorable source of tunable coherent infrared radiation for high-resolution direct-frequency-reading spectroscopy [2]–[4]. For linear absorption spectroscopy, wide-band tuning of the sideband is desired at a power level on the order of 100 μW. Whereas this power level is readily obtained by laser and microwave drive power levels of a few watts within CdTe- or GaAs-electrooptic crystals, tunability is restricted to some 10 GHz by microwave dispersion induced velocity mismatch of driving microwave and of modulated laser beam within conventional waveguiding structures [5].

Extremely broad-band light modulators operating at microwave frequencies call for a waveguide structure containing the electrooptic crystal at a location of maximum electric field and additionally for a velocity match over a broad frequency interval. With both respects, the double ridged waveguide shown in Fig. 1 seems promising. The electrooptic crystal is located between the ridges where, for dominant-mode operation, a desirable concentration of the microwave field is provided. On the other hand, one can expect to achieve velocity match for the laser beam and the microwave signal by judicious choice of waveguide dimensions. By the intrinsic parallel-plate line behavior of the double ridged waveguide, this velocity match is anticipated to hold for a wide frequency range.

In the following section we describe the electromagnetic field of the dominant mode in terms of a modal series expansion. The numerical evaluation of the unknown propagation constant is outlined in Section III. Section IV contains the comparison of measurements of the propagation constant with numerical results to check on the validity of our method. Design considerations and the evaluation of modulator efficiency and of bandwidth are presented in Section V.

II. Field Components

The electromagnetic field of the dominant mode will be described as a linear combination of the undisturbed field pattern of the dominant mode in a slab loaded rectangular waveguide [6], [7], and of higher order modes. The notation used will be the same as already given in [8], [16]. However, the hybrid character of the ridge guide modes will be accounted for by including both a longitudinal electric and a longitudinal magnetic field component.

For region I of the cross section ($-a' \leqslant x \leqslant 0$)—where the modulator crystal will be placed—the longitudinal field components of the dominant mode can be written as

$$E_{z1} = E_1 \exp(-jk_z z) \sum_{n=1}^{\infty} Q_n \operatorname{ch}(\Gamma_{n1}\xi_1) \sin(k_{yn1} y)$$

$$H_{z1} = E_1 (k_z/\omega\mu_1) \exp(-jk_z z) \cdot \left[\sin(k_{x1}\xi_1) + \sum_{n=1}^{\infty} R_n \operatorname{sh}(\Gamma_{n1}\xi_1) \cos(k_{yn1} y)\right]. \quad (1)$$

The corresponding field components of region II ($0 \leqslant x \leqslant (a-a')/2$) are expressed by

$$E_{z2} = E_2 \exp(-jk_z z) \sum_{n=1}^{\infty} S_n \operatorname{sh}(\Gamma_{n2}\xi_2) \sin(k_{yn2} y)$$

$$H_{z2} = E_2 (k_z/\omega\mu_2) \exp(-jk_z z) \cdot \left[\cos(k_{x2}\xi_2) + \sum_{n=1}^{\infty} T_n \operatorname{ch}(\Gamma_{n2}\xi_2) \cos(k_{yn2} y)\right]. \quad (2)$$

The remaining field components can be derived from (1) and (2) by insertion into Maxwell's equations.

The amplitudes of the undisturbed part of the electric field are denoted by E_i ($i=1,2$), whereas the relative amplitudes of the higher order modes are given by Q_n, R_n, S_n, and T_n, respectively. The wavenumbers in x-direction for the undisturbed and for the higher order part of the fields are denoted by k_{xi} and Γ_{ni}, respectively, and k_z is the propagation constant of the whole mode pattern in z-direction. The wavenumbers in y-direction are given by

$$k_{yn1} = 2n\pi/b'$$
$$k_{yn2} = 2n\pi/b \quad (3)$$

and the quantities ξ_i denote abbreviations for

$$\xi_1 = a'/2 + x$$
$$\xi_2 = (a-a')/2 - x. \quad (4)$$

Inserting (1) and (2) into the wave equation yields the separation conditions

$$k_{xi}^2 + k_z^2 = \omega^2 \epsilon_i \mu_i$$
$$-\Gamma_{ni}^2 + k_{yni}^2 + k_z^2 = \omega^2 \epsilon_i \mu_i. \quad (5)$$

The remaining equations necessary for the determination of the unknown amplitudes of the higher order modes are obtained by matching the tangential electromagnetic field components at $x=0$. As the sum of the higher order modes in (1) and (2) can be regarded as a Fourier series expansion in y-direction, their amplitudes can be calculated by the well-known deconvolution method already described in [9]. Evaluation of the zero-order Fourier coefficient of E_y

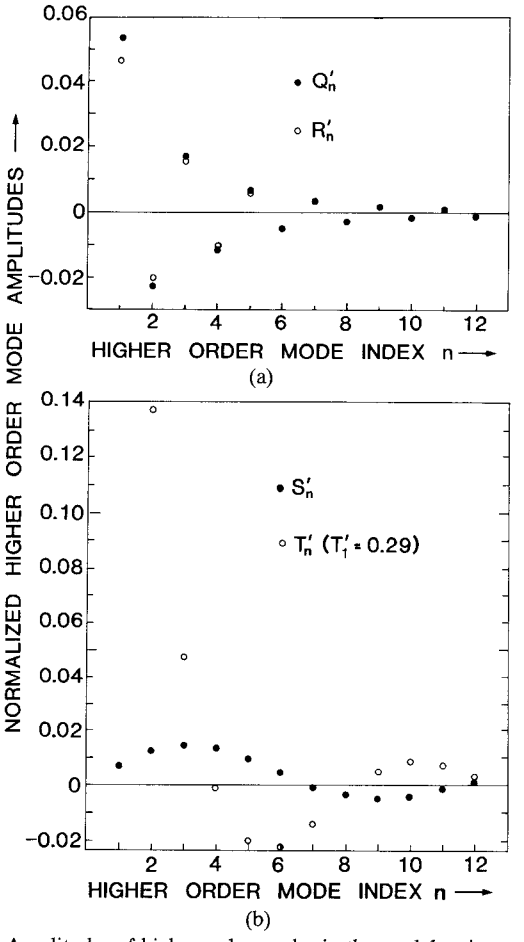

Fig. 2 Amplitudes of higher order modes in the modal series expansion of the dominant mode pattern. In particular, the amplitudes of the fringing electric (Q'_n, S'_n) and magnetic (R'_n, T'_n) field components at the dielectric–dielectric interface are shown for (a) region I, and (b) region II, of the cross section.

yields

$$E_2 = E_1 \cdot \frac{b' k_{x2} \cos(k_{x1} a'/2)}{b k_{x1} \sin(k_{x2}(a-a')/2)}. \tag{6}$$

The same procedure carried out for H_z results in the dispersion equation

$$\begin{aligned}(bk_{x1}\mu_2/b'k_{x2}\mu_1)\tan(k_{x1}a'/2) - \cot(k_{x2}(a-a')/2) \\ - [1/\sin(k_{x2}(a-a')/2)] \\ \cdot \sum_{n=1}^{\infty} T_n \operatorname{ch}(\Gamma_{n2}(a-a')/2)\operatorname{sinc}(n\pi b'/b) = 0.\end{aligned} \tag{7}$$

Extending the Fourier deconvolution to the higher order terms establishes a set of $4n$ linear equations from which the relative amplitudes Q_n, R_n, S_n, and T_n can be calculated. This set of equations is derived in the Appendix.

III. Numerical Evaluation

For any given frequency ω above cutoff the propagation constant k_z will be found within the interval $0 < k_z < \omega\sqrt{\epsilon_1 \mu_1}$. Dividing this interval by a set of 25 equally spaced values of k_z—which serve as first-order estimates—the remaining wavenumbers are calculated from (5). As a next step, we evaluate the higher order mode amplitudes Q_n, R_n, S_n, and T_n. Arranging the corresponding equations of the Appendix in the order (A.3), (A.2), (A.4), and (A.6) yields a system of $4n$ linear equations which are solved numerically by the Gaussian algorithm employing a partial search for the pivot element [10]. Now the T_n's are inserted into the dispersion equation (7). Whenever a zero of this equation is detected between two estimates of k_z, the ultimate value of k_z is approached by the method of bisection.

As the number N of higher order modes employed in the calculation influences both numerical accuracy and computer time, we have calculated the normalized higher order mode amplitudes as defined by (A.7) for several cross-sectional dimensions at frequencies ranging from 10 GHz to 50 GHz. An illustrative example is presented in Fig. 2, where Q'_n, R'_n, S'_n, and T'_n are shown for $n = 1, 2, \cdots, 12$. The cross-sectional dimensions of the ridged guide were chosen $a = 6$ mm, $b = 5$ mm, $a' = b' = 1.1$ mm, the relative permittivities $\epsilon_{r1} = 10.0$ (CdTe) and $\epsilon_{r2} = 1.0$, and the frequency $f = 30$ GHz. It should be noted that the normalized amplitudes are essentially the same over the frequency

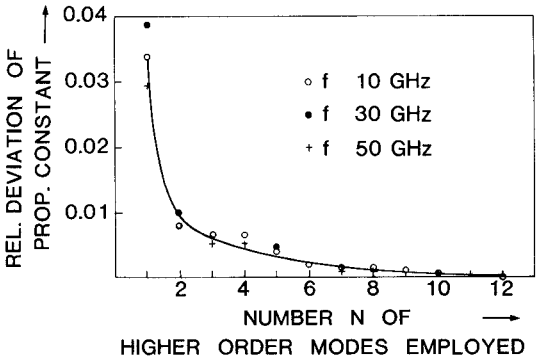

Fig. 3. Convergence of the propagation constant depending on the number N of higher order modes employed in the numerical calculation. Deviation is normalized to k_z numerically obtained for $N \geq 12$.

interval indicated above. The even more rapid convergence of k_z with increasing N is shown in Fig. 3. For identical waveguide parameters, the propagation constant k_z does not change significantly for $N \geq 12$. Even for $N=2$ an accuracy of about 1 percent is already achieved. Again, the frequency dependence is very weak.

IV. Measurements

To confirm the numerical results we investigated the propagation behavior of the dominant mode in an inhomogeneously dielectrically loaded double ridge waveguide. We chose the cross-sectional dimensions close to a conceivable modulator structure as $a=6.0$ mm, $b=5.0$ mm, and $a'=b'=1.1$ mm. The length of the waveguide was $L=91.6$ mm. As a replacement for the electrooptic crystal served an alumina slab (96 percent Al_2O_3, $a'=b'=1.1$ mm) with a relative permittivity of $\epsilon_{r1}=9.3$. Region II of the waveguide cross section remained empty ($\epsilon_{r2}=1.0$). To easily obtain reliable data on the wavelength, we designed the waveguide as a resonant cavity, one end short-circuited by a massive brass plate. Microwave energy was fed to the ridge guide resonator by face-to-face coupling to regular rectangular waveguides in the 8.2–12.4-GHz, 12.4–18.0-GHz, 18.0–26.5-GHz, and 26.5–40-GHz bands. The discontinuity at the feeding waveguide ridge guide boundary turned out to provide reasonable coupling over the whole frequency range investigated. At the microwave resonances of the ridge guide the unknown propagation constant was determined by

$$k_z = p\pi/L, \qquad p=6,7,8,\cdots,60 \tag{8}$$

neglecting any alteration of L due to fringing fields at the coupling plane.

Fig. 4 shows the dispersion diagram of the ridged guide. The dots represent the measured values of k_z according to (8), whereas the full line is obtained by numerically solving the dispersion equation (7). In the numerical solution six higher order modes were employed and the dielectric constant of the slab was chosen $\epsilon_{r1}=8$. No other fitting parameter was used. This decrease of the relative permittivity corresponds to an unavoidable air gap between the waveguide ridges and the alumina slab of thickness $t=0.02$ mm [11]. The deviations of measured and calculated values

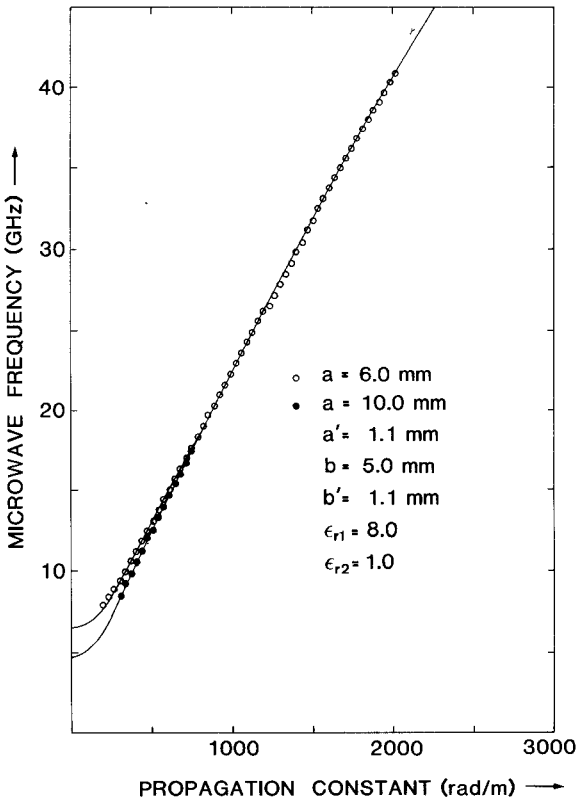

Fig. 4. Dispersion diagram of dielectrically loaded ridged waveguide. Measured values are indicated by dots.

are on the order of ± 0.2 percent over the whole frequency interval investigated. To confirm the apparent reduction of the dielectric constant we increased the waveguide width to $a=10$ mm with all other parameters remaining unchanged. Again, measurement and calculation coincide to within better than ± 0.5 percent as also can be seen from Fig. 4. Therefore, we can confidently rely on the modal description and on the numerical evaluation outlined above when designing a ridge-guide modulator.

V. Modulator Design

The power P_{SB} contained in one of the two lowest order sidebands generated from a laser carrier with power P_L is given by [12]

$$P_{SB} = P_L \Delta^2/16 \tag{9}$$

where the single-pass phase retardation Δ induced by the transverse electrooptic effect can be written as [13], [14]

$$\Delta = (2\pi/\lambda_0) n_0^3 r_{41} E_m L \operatorname{sinc}(\omega_m L/2w). \quad (10)$$

In (10), the symbol λ_0 stands for the free-space wavelength of the CO_2 laser, E_m denotes the electric microwave field strength within the modulator crystal, n_0 is the refractive index, r_{41} is the electrooptic coefficient, and L is the length of the modulator crystal. The abbreviation $\operatorname{sinc}(x)$ is used for $\sin(x)/x$, ω_m stands for the angular frequency of the modulating signal, and $1/w$ characterizes the mismatch of microwave phase (v_m) and of laser (v_L) group velocities within the modulator

$$1/w = 1/v_L - 1/v_m. \quad (11)$$

For maximizing the modulator efficiency we have to produce as much electric field strength as possible from a given amount of microwave drive power. In principle, this can be done by reducing the thickness (electrode separation) of the modulator. However, the RF impedance of such a device will decrease accordingly, and impedance matching to any conventional feeding line can be achieved only by bandwidth-limiting impedance transformers. On the other hand, the smallest cross section of commercially available modulator crystals is on the order of 1×1 mm^2. Therefore, we will assume this as a lower limit in our design considerations.

Choosing a long modulator crystal will boost the sideband intensity. However, benefit can be drawn from a long crystal only at low modulation frequencies ($\omega_m L/v_m \ll \pi$) or for perfect velocity match ($1/w = 0$) at any modulation frequency. As the double ridged waveguide has very little dispersion indeed (Fig. 4), we have investigated its usefulness as a CO_2-laser modulator. To provide exact velocity match in the 30–40-GHz range, we chose the cross-sectional dimensions as $a = 12.5$ mm, $b = 6.0$ mm, and $b' = 1.0$ mm. The width a' of the modulator crystal served as a parameter. The electrooptic material CdTe was chosen as modulator crystal with $n = 2.67$, $\epsilon_{r1} = 10.0$, and $n_0^3 r_{41} = 10^{-10}$m/V [15].

As a first step in the evaluation of (9) and (10), we calculated the propagation constant k_z and the microwave phase velocity $v_m = \omega_m/k_z$ within a frequency range from 10 GHz to 60 GHz. This enabled us to study the bandwidth limiting effects of microwave dispersion. Next, we computed the x- and y-dependence of the electric microwave field component E_{y1} assuming a microwave drive power of 1 W. It turned out that this field component exhibits an essentially uniform distribution over the modulator cross section. Even at the boundary of the modulator crystal ($x = 0$) still 80 percent of its maximum value at the center of the crystal is present. This favorable behavior justifies to insert the maximum value of E_{y1} in (10) for the modulating field strength E_m. Fig. 5 shows the sideband power generated from 1-W laser power by a traveling-wave modulator of $L = 25$ mm length. Decreasing the modulator

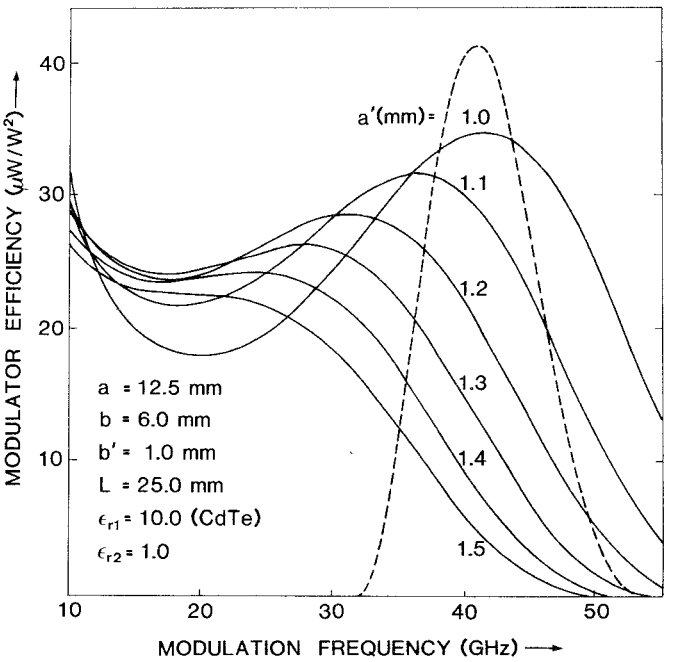

Fig. 5. Ridged-guide modulator efficiency, defined by sideband power generated from 1-W laser power at 1-W microwave drive power level, as a function of modulation frequency. For comparison, the performance of a conventional modulator (CdTe crystal of dimensions $a = 2.16$ mm, $b = 1.0$ mm, and $L = 25$ mm, completely enclosed in a fitting rectangular waveguide) is given by the dashed line.

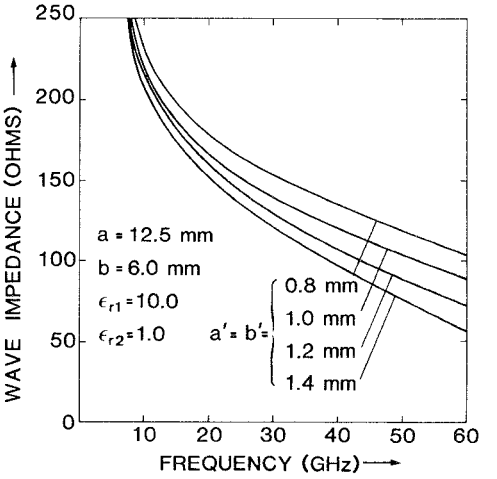

Fig. 6. Wave impedance of the dominant mode propagating in the double ridged waveguide.

width a' will increase sideband power along with the frequency where velocity match occurs, however, at the expense of sideband power at about 20 GHz. This can limit the usable 3-dB bandwidth. In the low-frequency regime two effects add favorably. First, any velocity mismatch becomes less detrimental due to the reduction of ω_m, compare (10), and—on the other hand—the modulating field strength rises in connection with the increasing wave impedance of the double ridged guide. Fig. 6 shows the wave impedance of the dominant mode as a function of frequency. For a quadratic modulator crystal cross section

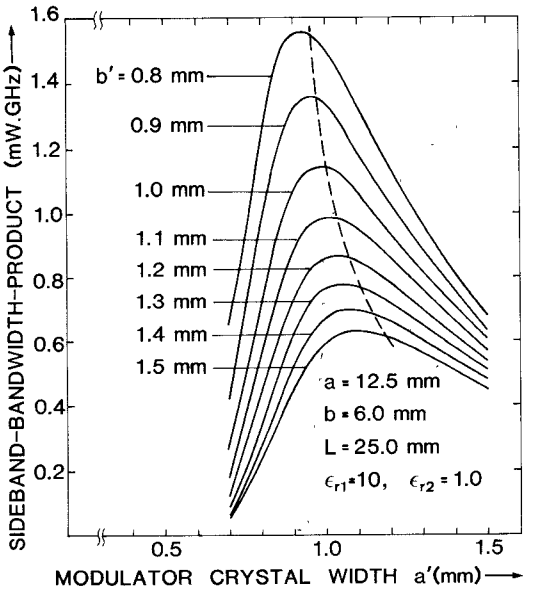

Fig. 7. Sideband–bandwidth product, defined by the area enclosed by the efficiency graph of Fig. 5 within 10 GHz and the frequency where a zero of sideband power occurs, for several cross-sectional geometries of the modulator crystal. Optimum crystal width a' for maximum 3-dB bandwidth is indicated by the dashed line.

with dimensions on the order of 1 mm, the wave impedance is about 130 Ω and shows little dispersion.

Turning back to Fig. 5, the bandwidth to be expected from a well-designed ridge-guide modulator is quite impressive. It extends over more than two octaves from 10 GHz to about 50 GHz for $a'=1$ mm. It should be pointed out that this bandwidth means not only tunability of a single-frequency sideband but also constitutes an instantaneous bandwidth for generating a broad sideband spectrum. For comparison, the sideband power generated by a conventional, 25-mm long modulator exhibiting the same velocity matching frequency is represented in Fig. 5 by a dashed line. This state-of-the-art modulator consists of an electrooptic crystal with dimensions of $a'=2.26$ mm and $b'=1$ mm completely enclosed in a rectangular waveguide [5]. Its peak sideband power is slightly higher than that of the ridge-modulator; its bandwidth, however, is only about 10 GHz as compared to 40 GHz of the ridge-guide modulator.

For spectroscopic purposes, a measure for the tunability of quite a modest sideband power level is even more important than 3-dB bandwidth. To establish such a measure we have calculated the area enclosed by the sideband-power graph within a frequency interval extending from 10 GHz to the frequency where the first zero of sideband power occurs. Again we assumed 1-W laser power and 1-W microwave drive power. This "sideband-bandwidth-product" is shown in Fig. 7. Generally, it increases with decreasing crystal height b'. However, there exists for every given crystal height b' an optimum value of crystal width a'. Interesting enough, this optimum clearly differs from the value of a' for maximum 3-dB bandwidth indicated by the dashed line in Fig. 7. For comparison, the sideband-bandwidth-product of our state-of-the-art modulator is about 0.43 mW·GHz.

VI. Conclusion

We have analyzed the dominant mode field of the inhomogeneously dielectrically loaded double ridged waveguide in terms of a higher order mode series expansion. From the continuity equations at the dielectric–dielectric boundary we have evaluated the propagation constant as a function of microwave frequency. The almost linear behavior of the dispersion diagram and the close agreement of measurements to calculation encouraged us to design an ultra-broad-band laser modulator based on the dielectrically loaded ridged guide. Bandwidth and sideband–bandwidth product were calculated to exceed the corresponding properties of any existing CO_2-laser modulator by far. In particular, a 3-dB bandwidth ranging from about 10 GHz to more than 50 GHz can be expected from a ridge-guide modulator.

Appendix

For the evaluation of the unknown higher order mode amplitudes Q_n, R_n, S_n, and T_n, a Fourier-series deconvolution of the continuity equations at the dielectric–dielectric boundary ($x=0$) is employed. Evaluating the zero-order Fourier coefficient of the electric field component E_y within the interval $-b/2 \leqslant y \leqslant b/2$ yields a relation between the undisturbed field amplitudes

$$E_2 = \eta E_1 \tag{A.1, a}$$

where the quantity η is defined by

$$\eta = [\beta k_{x2} \cos(k_{x1}\alpha_1)]/[k_{x1} \sin(k_{x2}\alpha_2)] \tag{A.1, b}$$

$$\alpha_1 = a'/2 \tag{A.1, c}$$

$$\alpha_2 = (a-a')/2 \tag{A.1, d}$$

and

$$\beta = b'/b. \tag{A.1, e}$$

Determination of the higher order Fourier coefficients yields ($k=1,2,\cdots$)

$$S_k k_{yk2} + T_k \Gamma_{k2} = -2k_{x2} \sin(k_{x2}\alpha_2) \operatorname{sinc}(k\pi\beta)/\operatorname{sh}(\Gamma_{k2}\alpha_2) + \left[k_{x2}^2 \beta/\left(k_{x1}^2 \eta \operatorname{sh}(\Gamma_{k2}\alpha_2)\right)\right]. \tag{A.2}$$

The same procedure applied to E_z at $x=0$ yields

$$S_k = (\beta\eta/\operatorname{sh}(\Gamma_{k2}\alpha_2)) \sum_{n=1}^{\infty} Q_n \operatorname{ch}(\Gamma_{n1}\alpha_1) \cdot [\operatorname{sinc}\pi(n-k\beta) - \operatorname{sinc}\pi(n+k\beta)]. \tag{A.3}$$

Now we turn to the tangential magnetic field components at the region I/region II boundary where for H_y

applies

$$R_k k_{yk1} - (\omega^2 \epsilon_1 \mu_1 / k_z^2) Q_k \Gamma_{k1} = \mu_1 k_{x1}^2 \eta / (\mu_2 k_{x2}^2 \mathrm{sh}(\Gamma_{k1}\alpha_1)) \cdot \sum_{n=1}^{\infty} \left(T_n k_{yn2} + (\omega^2 \epsilon_2 \mu_2 / k_z^2) S_n \Gamma_{n2}\right) \mathrm{ch}(\Gamma_{n2}\alpha_2) \cdot [\mathrm{sinc}\,\pi(k-n\beta) - \mathrm{sinc}\,\pi(k+n\beta)]. \quad (A.4)$$

Finally, we evaluate the zero-order Fourier coefficient of H_z resulting in the dispersion equation

$$[\mu_2 k_{x1}/(\mu_1 k_{x2}\beta)] \tan(k_{x1}\alpha_1) - \cot(k_{x2}\alpha_2) - (1/\sin(k_{x2}\alpha_2)) \cdot \sum_{n=1}^{\infty} T_n \mathrm{ch}(\Gamma_{n2}\alpha_2)\,\mathrm{sinc}(n\pi\beta) = 0 \quad (A.5)$$

and the higher order coefficients

$$R_k = [\eta\mu_1/(\mu_2 \mathrm{sh}(\Gamma_{k1}\alpha_1))] \sum_{n=1}^{\infty} T_n \mathrm{ch}(\Gamma_{n2}\alpha_2) \cdot [\mathrm{sinc}\,\pi(k+n\beta) + \mathrm{sinc}\,\pi(k-n\beta)]. \quad (A.6)$$

To gain insight in the relative magnitudes of the fringing fields, we calculate the higher order mode amplitudes at the location of their maximum ($x = 0$) and normalize them to the amplitude E_1 of the undisturbed field within the modulator crystal. This procedure results in the normalized higher order mode amplitudes shown in Fig. 2 which are defined by

$$Q_n' = Q_n \mathrm{ch}(\Gamma_{n1}\alpha_1) \quad (A.7, a)$$

$$R_n' = R_n \mathrm{sh}(\Gamma_{n1}\alpha_1) \quad (A.7, b)$$

$$S_n' = S_n \eta \,\mathrm{sh}(\Gamma_{n2}\alpha_2) \quad (A.7, c)$$

and

$$T_n' = T_n \eta \,\mathrm{ch}(\Gamma_{n2}\alpha_2). \quad (A.7, d)$$

ACKNOWLEDGMENT

The authors are indebted to Prof. E. Bonek for many stimulating discussions during the preparation of the manuscript. The computer center of the Technical University of Vienna provided free computer time.

REFERENCES

[1] C. Freed, L. C. Bradley, and R. G. O'Donnell, "Absolute frequencies of lasing transitions in seven CO_2 isotopic species," *IEEE J. Quantum Electron.*, vol. QE-16, pp. 1195–1206, 1980.

[2] V. J. Corcoran, J. M. Martin, and W. T. Smith, "Extension of microwave spectroscopy techniques to the infrared region," *Appl. Phys. Lett.*, vol. 22, pp. 517–519, 1973.

[3] J. Orr and T. Oka, "Doppler-free optical double resonance spectroscopy using a single-frequency laser and modulation sidebands," *Appl. Phys.*, vol. 21, pp. 293–306, 1980.

[4] G. Magerl, W. Schupita, E. Bonek, and W. A. Kreiner, "Direct frequency reading laser spectroscopy: ν_3 fundamental and stark effect of CH_3F," *J. Mol. Spectrosc.*, vol. 83, pp. 431–439, 1980.

[5] G. Magerl and E. Bonek, "Direct-Frequency-Reading IR spectroscopy," in *Proc. Int. Conf. LASERS '79*. McLean, VA: STS Press, pp. 732–738.

[6] F. Gardiol, "Higher-order modes in dielectrically loaded rectangular waveguides," *IEEE Trans. Microwave Theory Tech.*, vol. MTT-16, pp. 919–924, 1968.

[7] E. Bonek and G. Magerl, "Propagation characteristics of dielectrically loaded rectangular waveguides for laser beam modulators," *Arch. Elek. Übertragung*, vol. 28, pp. 499–506, 1974.

[8] G. Magerl, "Ridged waveguides with inhomogeneous dielectric-slab loading," *IEEE Trans. Microwave Theory Tech.*, vol. MTT-26, pp. 413–416, 1978.

[9] J. R. Whinnery and H. W. Jamieson, "Equivalent circuits for discontinuities in transmission lines," *Proc. IRE*, vol. 32, pp. 98–114, 1944.

[10] A. Wexler, "Computation of electromagnetic fields," *IEEE Trans. Microwave Theory Tech.*, vol. MTT-17, pp. 416–439, 1969.

[11] K. S. Champlin and G. H. Glover, "Gap-effect in measurement of large permittivities," *IEEE Trans. Microwave Theory Tech.*, vol. MTT-14, pp. 397–398, 1966.

[12] N. McAvoy, J. Osmundson, and G. Schiffner, "Broad-band CO_2 laser coupling modulation," *Appl. Opt.*, vol. 11, pp. 473–474, 1972.

[13] S. Namba, "Electro-optical effect of zincblende," *J. Opt. Soc. Amer.*, vol. 51, pp. 76–79, 1961.

[14] I. P. Kaminow and J. Liu, "Propagation characteristics of partially loaded two-conductor transmission line for broadband light modulators," *Proc. IEEE*, vol. 51, pp. 132–136, 1963.

[15] "CO_2 Laser Optics," *Data Sheets on Electrooptic Materials*, II–IV Inc., Saxonburg, 1979.

[16] C. W. Young and G. Magerl, "Comments on ridged waveguides with inhomogeneous dielectric-slab loading," *IEEE Trans. Microwave Theory Tech.*, vol. MTT-26, p. 919, 1978.

Gottfried Magerl (M'78) was born in Vienna, Austria, on August 16, 1947. He received both the Diplom-Ingenieur and the Doctor's degree from the Technische Universität Wien, Vienna, Austria, in 1972 and 1975, respectively.

Since 1973 he has been with the Institut für Nachrichtentechnik as a Research Associate and as an Assistant Professor. In 1980 he was appointed Academic Lecturer (Universitätsdozent) at the Technische Universität Wien. His professional interests include microwave measurements, guided electromagnetic wave propagation, microwave modulation of CO_2 lasers, and high-resolution molecular spectroscopy. At present, he is on leave of absence at the University of Chicago, Chicago, Illinois, to construct a laser sideband spectrometer at the Department of Chemistry.

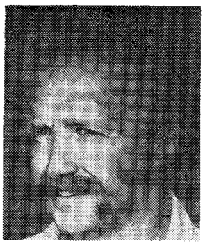

Peter W. Froehling was born in Vienna, Austria on December 27, 1952. He received the Diplom-Ingenieur degree in electrical engineering from the Technische Universität Wien, Vienna, Austria, in 1980 and is presently working toward the Ph.D.

Employed at the Institut für Nachrichtentechnik, his research interests include broad-band light modulators, electromagnetic field theory, and numerical methods.